Volume 17 Number 7 1989 Nucleic Acids Research

DNA topology of the ordered chromatin domain 5′ to the human c-*myc* gene

S.Kumar and M.Leffak

Department of Biochemistry, Wright State University, Dayton, OH 45435, USA

Received September 27, 1988; Revised and Accepted March 2, 1989

ABSTRACT

DNA restriction fragments located 5′ to the human c-*myc* gene display anomalous electrophoretic mobility on polyacrylamide gels. Computer modeling of the c-*myc* flanking DNA suggests that the slow-moving DNA fragments spanning nucleotides -1690 to -1054 (relative to c-*myc* promoter P_1) and -718 to -452 form large left handed superhelices or curved structures while the fast-moving DNA fragment spanning nucleotides -407 to +78 has an unusually straight structure. These analyses also predict a periodic array of localized regions of bending through the superhelical domains. Microccocal nuclease digestion of isolated nuclei reveals that the slow-moving DNA fragments exist in an ordered chromatin structure stable to nuclease, whereas the digestion pattern of the fast-moving DNA fragment suggests a less ordered array of nucleosomes or a non-nucleosomal chromatin structure.

INTRODUCTION

Stably curved DNA in solution was first detected by the anomalously slow electrophoretic migration of trypanosome kinetoplast DNA in polyacrylamide gels [1]. Such slowly migrating structures result when sequences capable of inducing a local structural polymorphism, for example A_n-tracts, are repeated in phase with the helix repeat [2–4]. Although the functional significance of curvilinear topology is incompletely understood, curved DNA has been found near elements important in transcription [5,6], recombination [7,8], and in the vicinity of sequences governing the replication of bacterial plasmids [9], bacteriophage lambda [10], SV40 [11,12], and yeast ARS elements [4,13–15]. That curved DNA may play a regulatory role in DNA replication is suggested by the observations that decreased binding of T-antigen to the SV40 origin region I [11] and inhibition of SV40 core replication origin activity [12] have been attributed to single-base mutations which alter the DNA curvature properties of these domains.

The curved DNA domain of the *Saccharomyces cerevisiae* ARS1 is essential for the activity of the replication enhancer element B [13,15,16], and Williams *et al.* have recently shown that synthetic A_n-tract DNAs can substitute for the bent DNA of element B [15]. In the case of a yeast TRP1ARS1 plasmid, nucleosomes are nonrandomly located

alongside the bipartite bent-straight DNA domain of the ARS1 element [17–19], consistent with suggestions that sequence directed curvature has the potential to influence chromatin structure by positioning nucleosome core particles through interaction with histone and non-histone chromosomal proteins [12,20–22]. Here we show that the 5′ flanking DNA of the human c-*myc* gene yields restriction fragments with anomalously slow or fast electrophoretic mobility in polyacrylamide gels. This region of DNA contains sequences which allow autonomous replication of plasmids in HeLa cells [23]. A computer program incorporating current models of sequence directed DNA curvature was used to generate helix trajectories. Fragments with reduced mobility were predicted to form large left-handed superhelices or simple bent structures, whereas the rapidly migrating fragments comprised unusually straight segments. Micrococcal nuclease digestion of isolated nuclei revealed an ordered set of cutting sites over one of the regions containing the curved DNA, reminiscent of a phased nucleosome array.

METHODS

Gel Electrophoresis

Three μg plasmid DNA (Figure 1A–C) containing the 2.5 Kb 5′ c-*myc* insert or the isolated insert (Figure 1D) was digested with the indicated restriction enzyme(s) (Bethesda Research Laboratories, New England Biolabs). Digested samples were mixed with 1 μg 123 bp ladder marker DNA (Bethesda Research Laboratories) and electrophoresed on 8% polyacrylamide slab gels in Tris-borate buffer [89*m*M Tris, 89*m*M Borate, 2*m*M Na-EDTA (pH 8.3)] at 4°C. Gels were stained with ethidium bromide and individual lanes excised. The excised lane was placed in the preparative well of a 1.2% agarose gel and electrophoresed in Tris-borate buffer with ethidium bromide at room temperature. Gels were photographed immediately after completion of electrophoresis. R_L values were calculated by comparing the apparent size of each restriction fragment (based on linear regression analysis of the marker ladder) to its actual size. R_L values have been rounded off to the nearest 0.05 unit.

Chromatin Analysis

The nuclei used in DNase I and MNase digestions were prepared from 3–5x10^7 HeLa cells as described by Siebenlist *et al.* [24]. Nuclei were digested at 37°C with MNase [10 U MNase / A_{260}] in nuclear isolation buffer [24] for the indicated times. Digestions were quenched with 10*m*M EGTA on ice. DNA was purified, digested with PstI, electrophoresed on 1.1% agarose gels in Tris-borate buffer, and transferred to Nytran (Schleicher & Schuell) membranes in 1M ammonium acetate. DNase I digestions were performed essentially as described by Siebenlist *et al.* [24] at the indicated concentrations of DNase I [U DNase I / ml] except that digestions were carried out for 6 minutes at room temperature. After purification, DNA was digested with XbaI and electrophoresed as described above and

transferred to Nytran membranes. Filters were hybridized in 6xSSC (1xSSC is 0.15 M NaCl, 0.015 M Na-citrate, pH 7.4), 0.5% SDS, 50% formamide, 200 μg/ml tRNA at 42°C. Probes were labelled with ^{32}P-dCTP by random primer extension. Stringency washes were with 0.2xSSC, 0.5% SDS at 65°C. Filters were exposed to Kodak X-Omat AR film at -80°C with intensifying screens.

Computer Modeling

The minimum energy 3D trajectory of the DNA helix was calculated using a chain-generating procedure described by Levene and Crothers [25]. Briefly, the coordinates of base pair n are computed in the coordinate system of base pair $n-1$, and then converted to a common world coordinate system, as follows: 1) establish a local coordinate system (right handed) [26] for an idealized base pair with coordinates $(x,y,z)_1$; 2) successively roll, tilt, twist (ρ, τ, Ω, respectively) and translate (rise Dz) [26] this base pair to get the local orientation of base pair n; 3) transform local coordinates to world coordinates. The information from previous tranforms is retained by compounding transformation matrices (using homogeneous coordinates). The initial transformation matrix is assumed to be the identity matrix. Steps 1-3 are repeated for each succeeding base pair. More succinctly,

$$(\,x \quad y \quad z\,)_n = [\,x \quad y \quad z \quad 1\,]_1 \left\{ \prod_{i=n-1}^{1} \begin{bmatrix} R_{i,i+1} & O_{3,1} \\ d_i & 1 \end{bmatrix} \right\} \begin{bmatrix} I_3 \\ O_{1,3} \end{bmatrix}$$

Where I and O represent identity and zero matrices, respectively, of the appropriate orders, and

$$d_i = [\,0 \quad 0 \quad Dz\,]$$

$$R_{i,i+1} = \begin{bmatrix} \cos\rho\cos\Omega - \sin\rho\sin\tau\sin\Omega & \cos\rho\sin\Omega + \sin\rho\sin\tau\cos\Omega & -\sin\rho\cos\tau \\ -\cos\tau\sin\Omega & \cos\tau\cos\Omega & \sin\tau \\ \sin\rho\cos\Omega + \cos\rho\sin\tau\sin\Omega & \sin\rho\sin\Omega - \cos\rho\sin\tau\cos\Omega & \cos\rho\cos\tau \end{bmatrix}$$

Roll, tilt, and twist parameters were dependent on the curve model chosen: wedge [27], junction-bend [28], Tung/Harvey [29], Dickerson/Calladine [30], Jernigan [31], Zhurkin [21], or Olson [32]. For simplification, where no sequence-specific twist parameter was specified, twist was obtained from the model of Kabsch *et. al.* [33]. Translational rise was kept constant at 0.34 nm. The program was written in VAXC and executed on a VAX 11/785 running under VMS 4.7. Stereo figures were drawn by separate FORTRAN programs incorporating DISSPLA (Integrated Software Systems Corp.) subroutines.

RESULTS

The 2.4 Kb region immediately 5′ to the human c-*myc* gene harbors sequence motifs implicated in the control of c-*myc* transcription *in vivo* and sites of protein binding *in vitro* (reviewed in [34-36]). Our laboratory has shown that this flanking DNA also serves as an ARS element in HeLa cells [23]. As recent studies have placed curved DNA in close

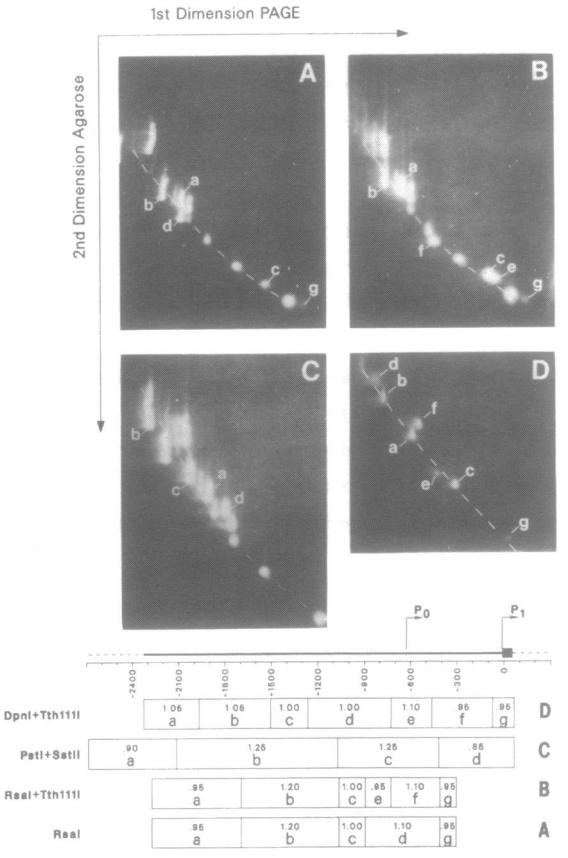

Figure 1 Separation of restriction fragments from a cloned portion of the 5′ flanking sequence of the human c-*myc* gene by 2D gel electrophoresis. A, RsaI; B, RsaI+Tth111I; C, PstI+SstII; D, DpnI+Tth111I. Electrophoresis in the first dimension (displayed horizontally) through 8% polyacrylamide at 4°C accentuated anomolies in mobility, allowing both size and shape factors to influence separation, whereas second dimension agarose electrophoresis (shown vertically) separated by size. A 123 bp DNA ladder was incorporated into the samples to provide a reference diagonal (approximated by the dashed line). Migration to the left of the diagonal indicated retarded mobility, while displacement to the right was indicative of enhanced mobility. R_L values (see text) were calculated from band mobilities and linear regression analysis of the marker ladder. Fragments not labelled in the figure are either part of the reference diagonal or are derived from vector sequences (fragments containing substantial amounts of vector sequences have been ignored in this study). A map of the c-*myc* locus is shown below the gels. Dashed lines represent vector sequences; the thick line is exon 1. Nucleotides are numbered relative to promoter P_1. The positions and R_L values of restriction fragments are displayed below the map.

proximity to replication origins, we sought to examine the topology of the 5′ c-*myc* region by exploiting the differential mobility of curved DNA in polyacrylamide versus agarose gels [1,4]. First dimension electrophoresis in 8% polyacrylamide gels at 4°C accentuates the anomalous behavior of curved DNA [3] and was used to separate fragments on the basis of size and shape. Separation by size alone was accomplished in the second dimension by agarose gel electrophoresis. A 123 bp ladder DNA marker incorporated into the samples served as the reference diagonal and for the calculation of R_L, the ratio of apparent to actual length [3].

For two-dimensional gel electrophoretic analysis, cloned c-*myc* DNA fragments were released from their plasmid vector by digestion with RsaI (Figure 1A), RsaI plus Tth111I (Figure 1B), or PstI plus SstII (Figure 1C). Alternatively, the isolated 2.4 Kb HindIII–XhoI fragment of c-*myc* 5′ flanking DNA was digested with DpnI plus Tth111I (Figure 1D). Two regions of significant curvature can be identified. The first spans nucleotide positions -718 to -452 (numbered relative to promoter P_1), in the vicinity of promoter P_0 [37] (Figures 1A–1D, fragments d, f, c, and e, respectively), while the second lies further upstream, betweeen -1690 nt and -1054 nt (fragment b, Figures 1A–1C). Restriction fragments completely overlapping these loci display R_L values between 1.1 and 1.3. While these values are smaller than those associated with kinetoplast DNA and synthetic A_n-tract oligonucleotides, they are comparable to the calculated R_L values for fragments containing the lambda origin [10] or SV40 origin [11] and yeast ARS elements [14].

Examination of the 2D gels also reveals a third region of c-*myc* that consistently migrates off the diagonal. Unlike the previous two regions, the region spanning -407 nt to +78 nt has a higher mobility than the reference standard (Figures 1A–D, fragments g, g, d, and f, respectively). Previous studies of DNA with anomalously high mobility have concluded that such fragments are apparently very straight, possessing little, if any, curvature [3,38]. Based on the models decribed below, the sequence of the 123 bp ladder marker system [39] predicts a slight curvature in the marker DNA (as in most natural DNAs examined; ref. [14]), thus forcing a slower migration in polyacrylamide gels than perfectly straight DNA fragments. Theoretical and empirical studies indicate that inherently straight sequences are less likely to wrap around the histone core [21,22; and references therein]. Therefore, fragments with R_L values less than 1.0, though generated by imperfect markers, may be indicative of regions that play a significant role in ordering chromatin structure.

Data obtained from gel mobility studies represent values averaged over the entire DNA fragment. A more precise, though theoretical, picture of the distribution of curvature is obtainable through computer analysis. Using parameters from published models of sequence dependent curvature [21,27–32], a program was constructed to calculate the

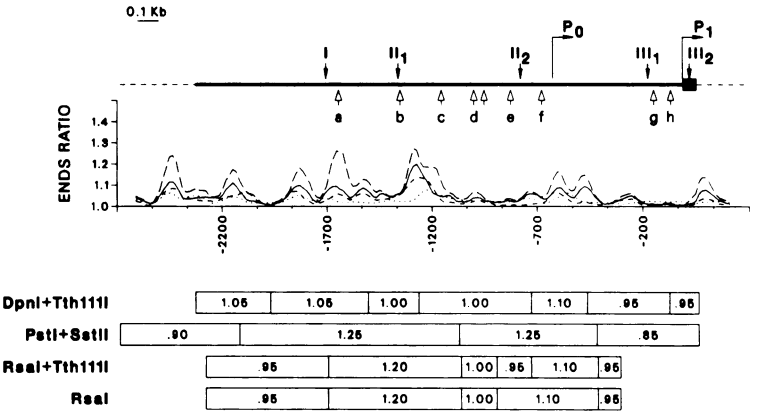

Figure 2 ENDS ratio plot over the 5′ flanking sequences of the c-*myc* locus. Using computed helix axis trajectories the ratio of contour length to direct end-to-end distance (ENDS ratio) [14] was calculated using a 150 bp sliding window. The vertical axis represents the ENDS ratio. The nucleotide position of the center of the sliding window is plotted on the horizontal axis. The positions and R_L values of restriction fragments are displayed below the ENDS ratio graph. Model assignments: ——, wedge; - - - - , junction-bend; ····· Olson, — —Jernigan. Other symbols are as described in previous figures.

predicted minimum-energy helix axis trajectory for the three regions displaying anomalous mobility. The calculated helix trajectory can be utilized to pinpoint regions of predicted

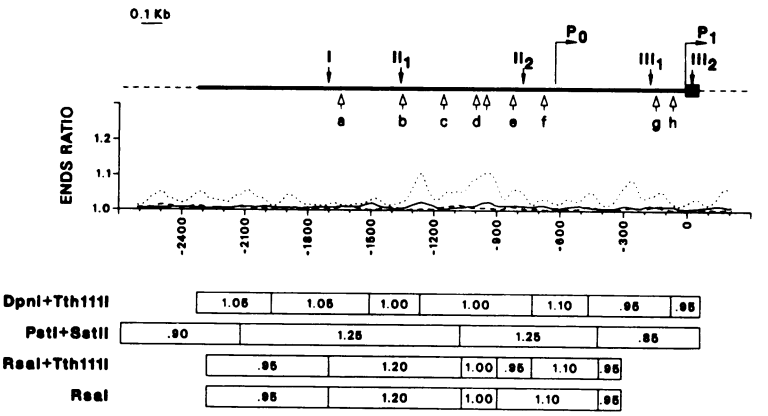

Figure 3 ENDS ratio plot over the 5′ flanking sequences of the c-*myc* locus. Model assignments: ——, Dickerson; - - - -, Tung/Harvey; ····· Zhurkin. See Figure 2 for explanation of symbols and methodology. Note that scale of the vertical axis is different from that of Figure 2 to accommodate the smaller ENDS ratio values in this plot.

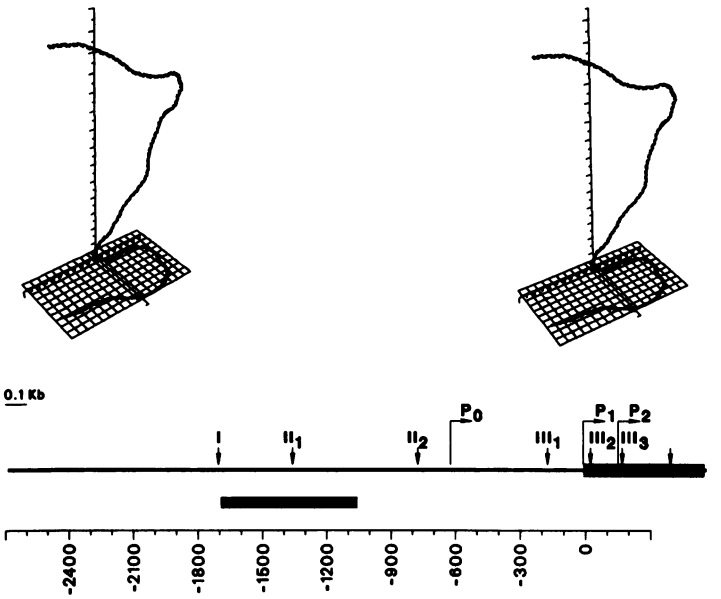

Figure 4 Stereo diagram of the computer modeling of 636 bp RsaI fragment b. Wedge model [27] parameters were used to calculate the DNA trajectory. The 5′ end of each fragment is located at the origin. Spacing between tick marks is 5 *n*m. A projection of the curve in the X-Y plane is drawn at the base of the graph. The thick bar below the c-*myc* map indicates the region being modeled. Other markings are as described in Figure 1.

maximum curvature by applying a sliding window calculation of the ENDS ratio (ratio of contour length to shortest length between two endpoints) over the entire sequence [14]. The positions of the predicted maxima are shown in Figures 2 and 3.

All models examined predicted the presence of curved DNA along the two regions that consistently show retardation of mobility in polacrylamide gels. However, the magnitude of the predicted curvature varied greatly between models. Such variation was also reported in the comparative bending analysis of Tan and Harvey [40]. Little or no significant curvature was predicted within the fragment that was believed to be essentially straight on the basis of gel mobility, with the exception of Zhurkin's model. None of the models match the gel data over *all* of the sequence. For example, over the extreme 5′ sequences and the region around -1000 nt, the predicted curvature is not manifested by elevated R_L values in polyacrylamide gels. Such discrepancies have been noted before [14] and are perhaps a reflection of the sensitivity of gel mobility to the position of curved sequences along DNA fragments [41].

Of the seven models implimented, the wedge and junction-bend models showed the

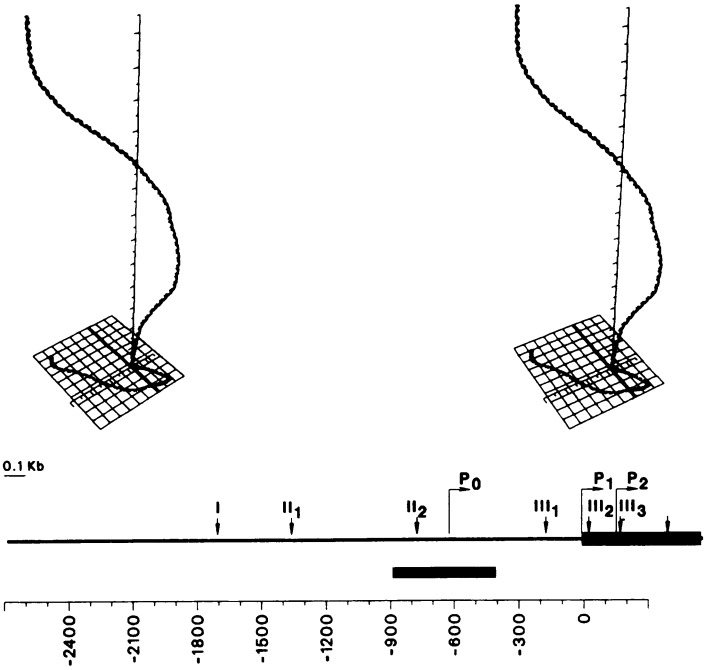

Figure 5 Stereo diagram of the computer modeling of 484 bp RsaI fragment d. See Figure 4 for explanation of symbols and methodology.

best agreement with the data obtained from the gel mobility analysis, though no single model was clearly superior to all others in this respect. The Dickerson and Tung/Harvey models appeared to underestimate DNA curvature and were therefore difficult to analyze. No effort was made to scale the roll/tilt values of the models for the purpose of comparison.

The wedge model was used to calculate the trajectories plotted in Figures 4–6. Figures 4 and 5 show as expected that the 637 bp and 484 bp RsaI fragments (Figure 1A, fragments b and d, respectively) are predicted to be curved, whereas Figure 6 predicts that the 486 bp PstI fragment (Figure 1C, fragment d) is composed of two very straight segments separated by a gentle curve. The 484 bp fragment, and to a lesser extent portions of the 637 bp fragment, form large left-handed superhelices, indicating the sequence elements responsible for the displayed curvature (in this case AA dinucleotides) are separated on average by slightly less than an integral multiple of the helix repeat. For comparison, the helix axis trajectories predicted by the other models that were examined are displayed in Figures 7 and 8 using a common coordinate system and constant viewpoint.

To determine if the curved topology 5′ of c-*myc* could be correlated with a unique

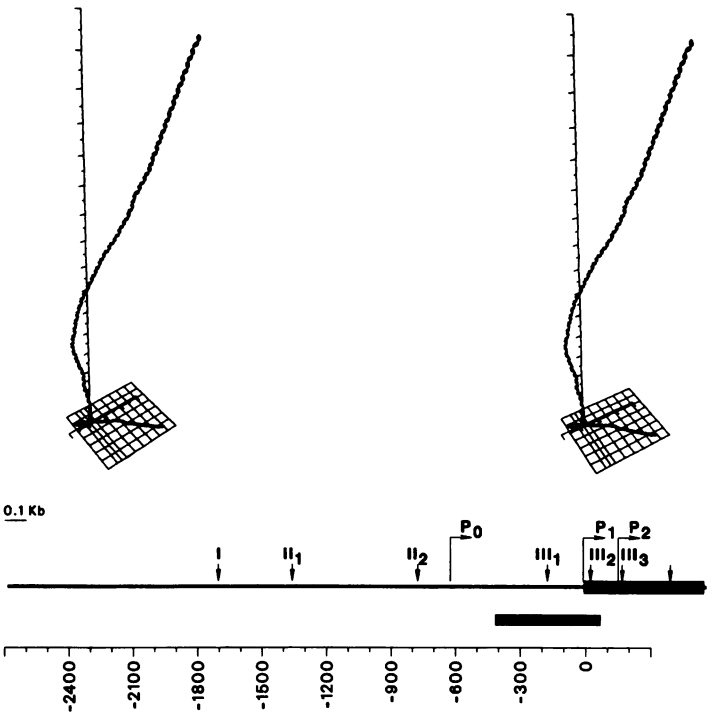

Figure 6 Stereo diagram of the computer modeling of 485 bp PstI fragment d. See Figure 4 for explanation of symbols and methodology.

chromatin structure, sites accessible to micrococcal nuclease (MNase) were mapped from the PstI site at -407 nt by indirect end-labelling. As shown in Figure 9A, the 1.7 Kb PstI fragment (P-P) from the 5′ flanking region is rapidly degraded into a set of discrete sub-fragments that are relatively resistant to further digestion. Control digestions of purified HeLa DNA did not yield a comparable set of fragments (data not shown). While the average nucleosome spacing in HeLa chromatin is ca. 195 bp, regularly spaced MNase cutting sites over the region -1400 nt to -600 nt were separated on average by ca. 150 bp, reminiscent of ladders obtained from MNase digestion of phased nucleosome arrays [42]. In contrast, analysis of the region 3′ to -407 nt showed that the same ordered chromatin structure does not extend over the domain which is predicted to have an inherently straight structure (Figure 9B). With the exception of a few closely spaced sites in exon 1, the digestion products of the parent 2.7 Kb PstI fragment migrate as a uniform smear. DNase I hypersensitive sites over the 5′ c-*myc* region were mapped by indirect end-labelling from the XbaI site using the 667 bp PvuII–XbaI fragment as the probe. The positions of

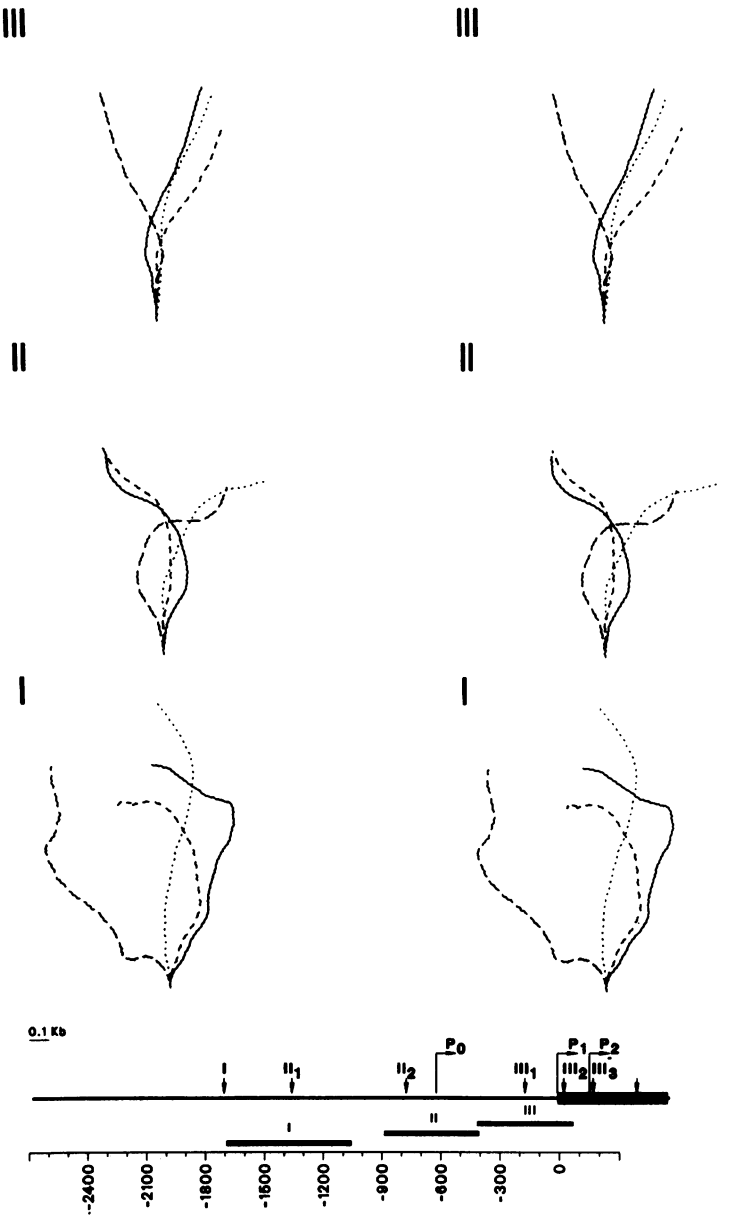

Figure 7 Stereo diagrams of the computer modeling of restriction fragments displaying anomalous mobility. (I) 636 bp RsaI fragment b. (II) 483 bp RsaI fragment d. (III) 485 bp PstI fragment d. Each set of curves is plotted on a common coordinate system with the 5′ end of each fragment located at the base. The viewing angle is parallel to the X–Y plane rather than at an angle as in Figures 4–6. Model assignments are identical to those in Figure 2.

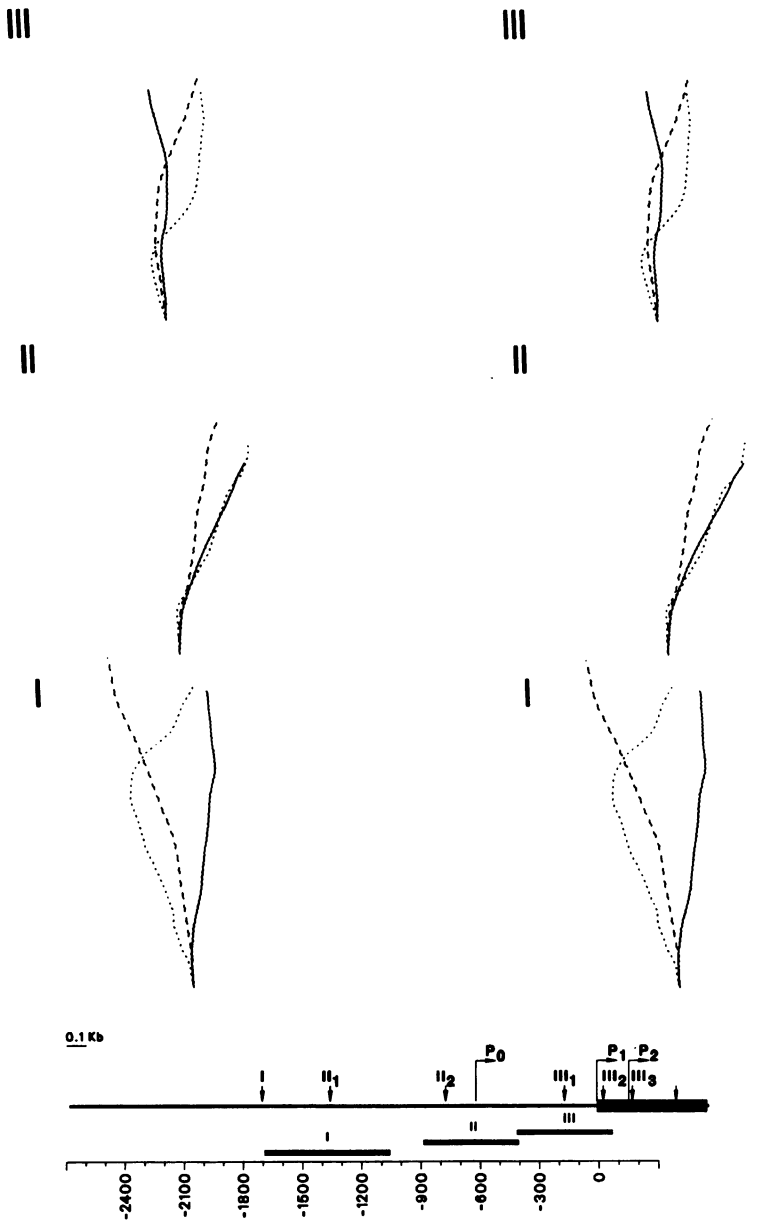

Figure 8 Stereo diagrams of the computer modeling of restriction fragments displaying anomalous mobility. Model assignments are identical to those in Figure 3. See Figure 7 for explanation of methodology and other symbols.

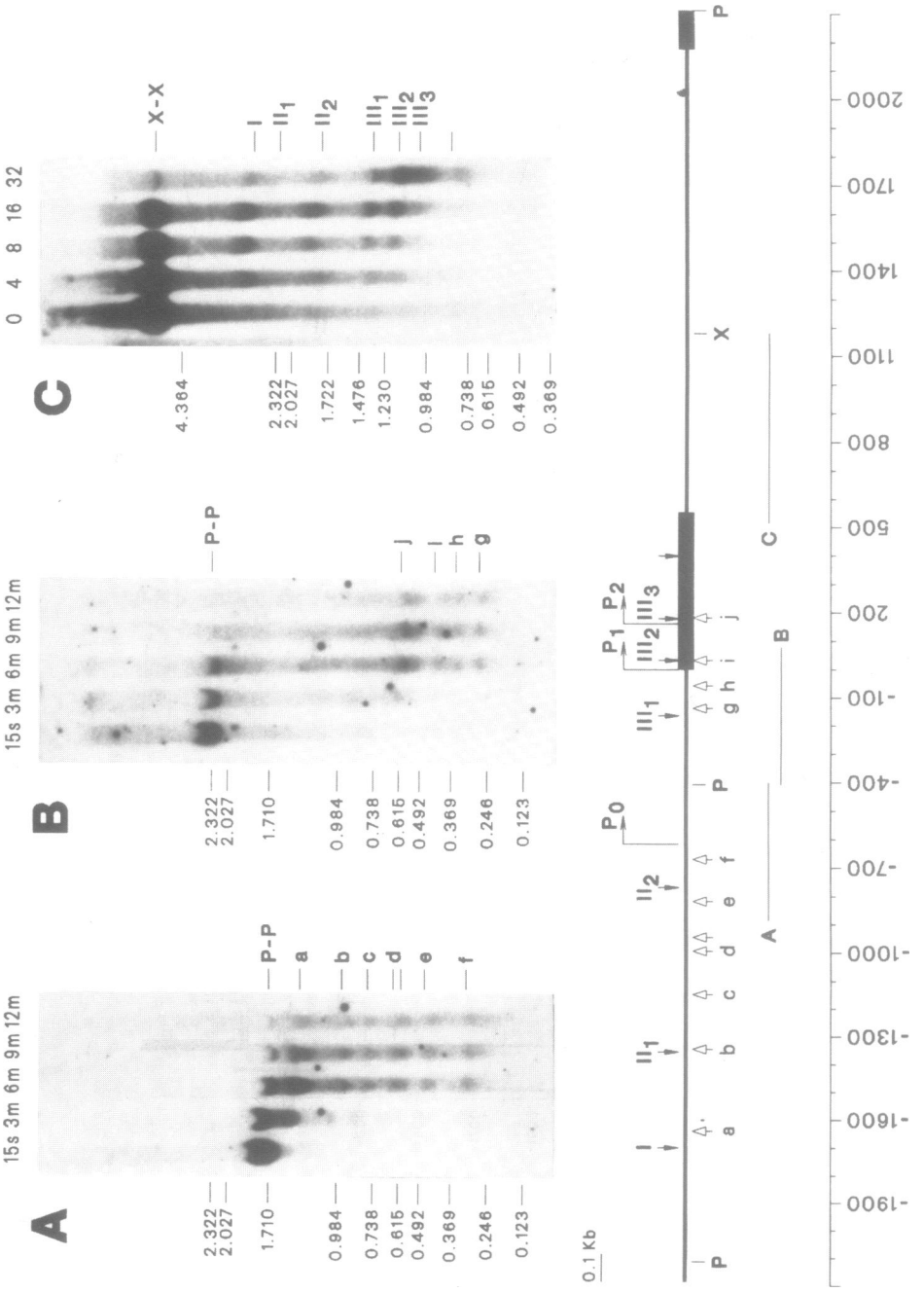
A
15s 3m 6m 9m 12m
2.322
2.027
1.710
0.984
0.738
0.615
0.492
0.369
0.246
0.123
P-P
a
b
c
d
e
f
B
15s 3m 6m 9m 12m
P-P
2.322
2.027
1.710
0.984
0.738
0.615
0.492
0.369
0.246
0.123
j
i
h
g
C
0 4 8 16 32
X-X
4.364
2.322
2.027
1.722
1.476
1.230
0.984
0.738
0.616
0.492
0.369
I
II1
II2
III1
III2
III3
0.1 Kb
P
I
II1
II2
P0
P1
P2
III1
III2
III3
a b c d e f
P
g h i j
X
A
B
C
2000
1700
1400
1100
800
500
200
-100
-400
-700
-1000
-1300
-1600
-1900

hypersensitive sites I–III identified for the HeLa cell line in Figure 9C correspond to those previously established for transcriptionally active c-*myc* genes in human cell lines 8392, PF, BL31, and HL60 [24,43,44]. Site II_1 was very, weak as in previous reports, but was consistently visible in the original autoradiographs. The weak site at the 3′ end of exon 1 was left unlabelled to correspond with the nomenclature of Siebenlist *et.al.* [43].

DISCUSSION

The 5′ flanking DNA of the human c-*myc* gene displays certain features common to yeast ARS elements in general [4,13–15] and the TRP1ARS1 plasmid in particular [17,18], namely the presence of sequences capable of permitting autonomous plasmid replication, a pattern of neighboring straight and superhelically curved segments, and the occurrence of an ordered chromatin structure. Experiments to pinpoint the location of the ARS within the c-*myc* flanking DNA are in progress, and preliminary data suggest that this element is located within ca. 2 Kb upstream of P_1 [C. McWhinney and M.L. ; unpublished data]. The c-*myc* ARS domain is similar to the yeast TRP1ARS1 plasmid in displaying an ordered chromatin structure near the ARS element [17,18]. The two differ in that the ordered chromatin structure appears to extend over the curved c-*myc* DNA, whereas the TRP1ARS1 curved DNA sequences reside in a region of nuclease hypersensitivity. This contrast may not be significant, however, in view of the variability within *S. cerevisiae* of the sizes of ARS-associated curved DNA domains and of their location relative to the ARS consensus [14].

Juxtaposition of the data from MNase mapping, gel mobility, and mathematical modeling (Figure 2) reveals that the DNA helix is significantly curved immediately 3′ to the

Figure 9 Mapping of MNase and DNase I cutting sites by indirect end-labelling. A and B. HeLa nuclei were digested for increasing times with MNase. DNA was purified, cut with PstI, electrophoresed and blotted to nylon membranes. The positions of MNase cutting in the 5′ direction relative to the PstI site at -407 nt (A), were determined by hybridization with the ^{32}P-labelled 483 bp RsaI fragment. Double lines and double arrows were used to label site d to indicate that the site was broad, appearing as a closely spaced doublet on autoradiographs of higher resolution gels (not shown). The sliding-end-labelling technique was applied to confirm that fragments smaller than the probe length were not generated by two internal MNase cuts [45] (not shown). MNase sites were mapped from the same site but in the 3′ direction (B) using a 385 bp PstI fragment as the probe. The 3′ PstI site of this fragment is derived from the vector sequence, 12 bp of which remain at its 3′ end. DNase I digestions (C) were carried out with increasing amounts of enzyme as described in ref. 24. After purification, DNA was digested with XbaI and the hypersensitive sites mapped by indirect end-labelling using the 657 bp PvuII–XbaI fragment as the probe. The sequences used as probes are indicated by thin lines below the region map. Open arrows indicate MNase cutting sites. Closed arrows mark DNase I hypersensitive sites. Other markings are as described in Figure 1.

first and last members of the 150 bp positioned subset of MNase cutting sites (MNase sites b through f). It is tempting to speculate that the curved topology 5′ to c-*myc* serves as a boundary signal for the formation of the ordered chromatin structure, analogous to the influence of flanking nuclease-sensitive regions on the positioning of nucleosomes over the TRP1 gene in TRP1ARS1 plasmids shown by Thoma [19]. However, within the same plasmid, Thoma and Simpson [18] concluded that nucleosome positioning over the UNF region [19] was the result of specific protein-DNA interactions, rather than simple boundary effects. That curved DNA represents a portion of the high-affinity binding sites for SV40 T-antigen [11] and the *Crithidia fasciculata* nicking enzyme [8] is consistent with the idea that DNA topology *per se* can contribute to site specific protein binding. In this regard, the periodic modulation of the ENDS ratio and the large number of potential protein binding sites recognized within the c-*myc* 5′ DNA [34,35] suggest that the ordered chromatin packaging of this region may play a role in replication as well as transcription.

ACKNOWLEDGEMENTS

We thank D. Crothers for kindly providing updated parameters for the junction--bend model prior to publication, and P. Leder for the phage clone of human c-*myc* DNA. We also thank S. Harvey for helpful comments and discussion on the computer modeling. Restriction maps and DNA sequences were obtained from the BIONET National Computer Resource for Molecular Biology which is funded by the Biomedical Research Technology Program, Division of Research Resources, National Institutes of Health, Grant Number P41RR01685. This work was supported by grants from the NIH (GM35877) and the American Cancer Society to M.L.

REFERENCES

1. Marini, J.C., Levene, S.D., Crothers, D.M. and Englund, P.T.(1982) *Proc. Natn. Acad. Sci. USA* **79**, 7664–7668.
2. Trifonov, E.N.(1986) *CRC Crit. Rev. Biochem.* **19**, 89–106.
3. Koo, H.S., Wu, H.M. and Crothers, D.M.(1986) *Nature* **320**, 501–506.
4. Anderson, J.N.(1986) *Nuc. Acids Res.* **14**, 8513–8533.
5. Bossi, L. and Smith, D.M.(1984) *Cell* **39**, 643–652.
6. Gourse, R.L., deBoer, H.A. and Nomura, M.(1986) *Cell* **44**, 197–205.
7. Ross, W., Shulman, M. and Landy, A. (1982) *J. Mol. Biol.* **156**, 505–529.
8. Linial, M. and Shlomai, J.(1987) *Proc. Natn. Acad. Sci. USA* **84**, 8205–8209.
9. Koepsel, R.R. and Khan, S.A. (1986) *Science* **233**, 1316–1318.
10. Zahn, K. and Blattner, F.R.(1985) *Nature* **317**, 451–453.
11. Ryder, K., Silver, S., DeLucia, A.L., Fanning, E. and Tegtmeyer, P.(1986) *Cell* **44**, 719–725.
12. Deb, S., DeLucia, A.L., Koff, A., Tsui, S., and Tegtmeyer, P. (1986) *Mol. Cell. Biol.* **6**, 4578–4584.
13. Snyder, M., Buchman, A.R., and Davis, R.W.(1986) *Nature* **324**. 87–89.

14. Eckdahl, T.T. and Anderson, J.N. (1987) *Nuc. Acids Res.* **15**, 8531–8545.
15. Williams, J.S., Eckdahl, T.T. and Anderson, J.N. (1988) *Mol. Cell. Biol.* **8**, 2763–2769.
16. Srienc, F., Bailey, J.E., and Campbell, J.L. (1985) *Mol. Cell. Biol.* **5**, 1676–1684.
17. Thoma, F., Bergman, L.W. and Simpson, R.T. (1984) *J. Mol. Biol.* **177**, 715–733.
18. Thoma, F. and Simpson, R.T. (1985) *Nature* **315**, 250–252.
19. Thoma, F. (1986) *J. Mol. Biol.* **190**, 177–190.
20. Griffith, J., Bleyman, M., Rauch, C.A., Kitchin, P.A. and Englund, P.T. (1987) *Cell* **46**, 717–724.
21. Zhurkin, V.B. (1985) *J. Biomol. Struct. Dyn.* **2**, 785–804.
22. Drew, H.R. and Travers, A.A. (1985) *J. Mol. Biol* **186**, 773–790.
23. McWhinney C. and Leffak, M. (1988) *Cancer Cells* **6**, 467–471.
24. Siebenlist, U., Hennighausen, L., Battey, J. and Leder, P. (1984) *Cell* **37**, 381–391.
25. Levene, S.D. and Crothers, D.M. (1983) *J. Biomol. Struct. Dyn.* **1**, 429–435.
26. Sarma, R.H. (1988) *J. Biomol. Struct. Dyn.* **6**, 391–395.
27. Ulanovsky, L.E. and Trifonov, E.N. (1987) *Nature* **326**, 720–722.
28. Koo, H.S. and Crothers, D.M. (1988) *Proc. Natn. Acad. Sci. USA* **85**, 1763–1767.
29. Tung, C.S. and Harvey, S.C. (1986) *J. Biol. Chem.* **261**, 3700–3709.
30. Dickerson, R.E. (1983) *J. Mol. Biol.* **166**, 419–441.
31. Jernigan, R.L., Sarai, A., Ting, K.L. and Nussinov, R. (1986) *J. Biomol. Struct. Dyn.* **4**, 41–48.
32. Srinivasan, A.R., Torres, R., Clarck, W. and Olson, W.K. (1987) *J. Biom. Struct. Dyn.* **5**, 459–496.
33. Kabsch, W., Sander, C. and Trifonov, E.N. (1982) *Nuc. Acids Res.* **10**, 1097–1104.
34. Chung, J., Sinn, E., Reep, R.R. and Leder, P. (1986) *Proc. Natn. Acad. Sci. USA* **83**, 7918–7922.
35. Lipp, M., Schilling, R., Wiest, S., Laux, G. and Bornkamm, G. (1987) *Mol. Cell. Biol.* **7**, 1393–1400.
36. Piechaczyk, M., Blanchard, J.M. and Jeanteur, P. (1987) *Trends Genet.* **3**, 47–51.
37. Bently, D.L. and Groudine, M. (1986) *Mol. Cell. Biol.* **6**, 3481–3489.
38. Diekmann, S. (1987) *EMBO* **6**, 4213–4217.
39. Hartley, J.L. and Gregori, T.J. (1981) *Gene* **13**, 347–353.
40. Tan, R. and Harvey, S.C, (1987) *J. Biom. Struct. Dyn.* **5**, 497–507.
41. Wu, H. and Crothers, D.M. (1984) *Nature* **308**, 509–513.
42. Wu, C. (1980) *Nature* **286**, 854–860.
43. Siebenlist, U., Bressler, P. and Kelly, K. (1988) *Mol. Cell. Biol.* **8**, 867–874.
44. Bentley, D.L. and Groudine, M. (1986) *Nature* **321**, 702–706.
45. Pérez-Ortín, J.E., Estruch, F., Matallana, E. and Franco, L. (1986) *FEBS Lett.* **208**, 31–33.